AFRL-VA-WP-TP-2006-327

ABLATION MODELING FOR DYNAMIC SIMULATION OF REENTRY VEHICLES (PREPRINT)

David B. Doman and William Blake

JULY 2006

Approved for public release; distribution is unlimited.

STINFO COPY

AIR VEHICLES DIRECTORATE
AIR FORCE MATERIEL COMMAND
AIR FORCE RESEARCH LABORATORY
WRIGHT-PATTERSON AIR FORCE BASE, OH 45433-7542

NOTICE AND SIGNATURE PAGE

AFRL-VA-WP-TP-2006-327 HAS BEEN REVIEWED AND IS APPROVED FOR PUBLICATION IN ACCORDANCE WITH ASSIGNED DISTRIBUTION STATEMENT.

*//Signature//

David B. Doman
Senior Aerospace Engineer
Control Design and Analysis Branch
Air Force Research Laboratory
Air Vehicles Directorate

//Signature//

Deborah S. Grismer
Chief
Control Design and Analysis Branch
Air Force Research Laboratory
Air Vehicles Directorate

//Signature//

JEFFREY C. TROMP
Senior Technical Advisor
Control Sciences Division
Air Vehicles Directorate

This report is published in the interest of scientific and technical information exchange, and its publication does not constitute the Government's approval or disapproval of its ideas or findings.

*Disseminated copies will show "//Signature//" stamped or typed above the signature blocks.

REPORT DOCUMENTATION PAGE

Form Approved
OMB No. 0704-0188

1. REPORT DATE *(DD-MM-YY)*	2. REPORT TYPE	3. DATES COVERED *(From - To)*
July 2006	Conference Paper Preprint	11/01/2004– 06/30/2006

4. TITLE AND SUBTITLE
ABLATION MODELING FOR DYNAMIC SIMULATION OF REENTRY VEHICLES (PREPRINT)

5a. CONTRACT NUMBER
In-house

5b. GRANT NUMBER

5c. PROGRAM ELEMENT NUMBER
62201F

6. AUTHOR(S)
David B. Doman and William B. Blake

5d. PROJECT NUMBER
A03D

5e. TASK NUMBER

5f. WORK UNIT NUMBER
0B

7. PERFORMING ORGANIZATION NAME(S) AND ADDRESS(ES)

Control Design and Analysis Branch (AFRL/VACA)
Control Sciences Division
Air Vehicles Directorate
Air Force Materiel Command, Air Force Research Laboratory
Wright-Patterson Air Force Base, OH 45433-7542

8. PERFORMING ORGANIZATION REPORT NUMBER
AFRL-VA-WP-TP-2006-327

9. SPONSORING/MONITORING AGENCY NAME(S) AND ADDRESS(ES)

Air Vehicles Directorate
Air Force Research Laboratory
Air Force Materiel Command
Wright-Patterson Air Force Base, OH 45433-7542

10. SPONSORING/MONITORING AGENCY ACRONYM(S)
AFRL-VA-WP

11. SPONSORING/MONITORING AGENCY REPORT NUMBER(S)
AFRL-VA-WP-TP-2006-327

12. DISTRIBUTION/AVAILABILITY STATEMENT
Approved for public release; distribution is unlimited.

13. SUPPLEMENTARY NOTES
This work has been submitted to the 2006 AIAA Guidance, Navigation, and Control Conference proceedings.
Report contains color. PAO Case Number: AFRL/WS 06-1787 (cleared July 19, 2006).

14. ABSTRACT

The collection of methods described in this manuscript can be used in a dynamic simulation to provide estimates of the mass properties and aerodynamic forces and moments as a reentry vehicle ablates due to aerodynamic heating. Vehicles that experience relatively low peak heating with reusable thermal protection systems such as the shuttle, experience little if any ablation. At the other extreme, ballistic reentry vehicles and interplanetary probes can experience very high peak heat loads that cause the thermal protection material to ablate. A number of vehicle characteristics change as a result of ablation. The mass properties of the vehicle change due to the loss of material and the aerodynamic forces and moments acting on the vehicle change as a result of the an ablating outer mold line (OML). These changes can affect aerodynamic as well as guidance and control system performance. Empirical methods are described in this paper that can be used to translate limited test data into a rough, but representative model that can be used to estimate the effects of ablation on a vehicle's ability to follow a prescribed trajectory and on guidance and control performance and robustness.

15. SUBJECT TERMS
Ablation, Reentry Vehicles, Dynamic Simulation

16. SECURITY CLASSIFICATION OF:			17. LIMITATION OF ABSTRACT:	18. NUMBER OF PAGES	19a. NAME OF RESPONSIBLE PERSON (Monitor)
a. REPORT	b. ABSTRACT	c. THIS PAGE			David B. Doman
Unclassified	Unclassified	Unclassified	SAR	24	19b. TELEPHONE NUMBER *(Include Area Code)* N/A

Standard Form 298 (Rev. 8-98)
Prescribed by ANSI Std. Z39-18

Ablation Modeling for Dynamic Simulation of Reentry Vehicles

David Doman* and William Blake†

Air Force Research Laboratory/VACA, Wright-Patterson AFB, OH 45433-7531

I. Introduction

The collection of methods described in this manuscript can be used in a dynamic simulation to provide estimates of the mass properties and aerodynamic forces and moments as a reentry vehicle ablates due to aerodynamic heating . Dynamic simulations of reentry vehicles are required to perform trajectory optimization and to analyze the robustness of guidance and control systems. Reentry vehicle trajectories vary widely depending on mission requirements and vehicle design. Vehicles that experience relatively low peak heating with reusable thermal protection systems such as the shuttle, experience little if any ablation. At the other extreme, ballistic reentry vehicles and interplanetary probes can experience very high peak heat loads that cause the thermal protection material to ablate. A number of vehicle characteristics change as a result of ablation. The mass properties of the vehicle change due to the loss of material and the aerodynamic forces and moments acting on the vehicle change as a result of the an ablating outer mold line (OML). These changes can affect aerodynamic as well as guidance and control system performance. A number of techniques exist that allow one to measure the changes to the OML[1,2] during experimental testing. Empirical methods are described in this paper that can be used to translate limited test data into a rough, but representative model that can be used to estimate the effects of ablation on a vehicle's ability to follow a prescribed trajectory and on guidance and control performance and robustness.

Section II proposes a method to estimate the location of points on the OML that lie outside of the vehicle plane of symmetry where test measurements are typically obtained. These points can be used to generate a 3 dimensional grid that is suitable for use with aerodynamic prediction codes. The out-of-plane grid points are estimated using a radial interpolation method that can accommodate asymmetries that occur between the windward and leeward surfaces of the vehicle . Formulae for the geometric properties of radially interpolated ablated nose cone profiles are provided.

Section III proposes a method to estimate the instantaneous mass of the nose cone that is suitable for use in a dynamic simulation. In Section IV, a method is described that allows one to estimate the location of the OML and aerodynamic coefficients between test or prediction points, based on the instantaneous mass. In Section V we describe the method used to generate the aerodynamic models for the example body described in Section VI.

II. Generation of Outer Mold Lines from Test Data

In order to generate an aerodynamic model of an ablated vehicle, an approximation for the outer mold line must be constructed. The shape of nose-cones from experimental recession measurements are often provided in the form of upper and lower curves that describe the surface of the body in the nominal plane of symmetry, i.e the body x-z plane. One objective of this section is to develop a method of estimating out-of-plane grid points so that an aerodynamics prediction or CFD code can be used to estimate the aerodynamic characteristics . For cases where only 2-D profiles are obtained from recession measurements, OML grid

*Senior Aerospace Engineer, AFRL/VACA, 2210 Eight Street, Bldg 146,Wright-Patterson AFB, OH. 45433-7531, Associate Fellow AIAA, david.doman@wpafb.af.mil

†Senior Aerospace Engineer, AFRL/VACA, 2210 Eight Street, Bldg 146,Wright-Patterson AFB, OH. 45433-7531, Associate Fellow AIAA, william.blake@wpafb.af.mil

points outside of the x-z plane must be estimated. The method presented here was developed for nose cones that are axissymmetric before ablation occurs.

Here we propose to estimate out-of-plane grid points by interpolating between two surfaces of revolution about the x-body axis. Figure 1 shows how the upper and lower curves defining a body in the x-z plane can be used to generate an interpolated body that can be used to obtain estimates of OML coordinates in the y-z plane.

Figure 1 shows a side and sectional view of a nose cone. The requirements are that the interpolated OML must be coincident with the upper curve when $\theta = \pi/2$ and with the lower curve when $\theta = -\pi/2$, where θ is the angle (in the y-z plane) measured from the y-axis to a point on one of the surfaces. Furthermore, the interpolated crossections are taken to be smooth at $\theta = \pm\pi/2$ and symmetric about the x-z plane. These boundary conditions are motivated by the fact that the OML of the unablated vehicle could be described by a surface of revolution. For lifting reentry vehicles, test data shows that leeward surfaces ablate less than the windward surfaces. Thus, the vehicle OML does not remain symmetric when flying at a non-zero angle-of-attack under thermal conditions where ablation occurs. We now construct an interpolation function that satisfies the position and slope boundary conditions described above.

Let $\lambda(\theta) \in [0, 1]$ be an interpolating function such that:

$$r_i(\theta) = \lambda(\theta) r_u + [1 - \lambda(\theta)] r_l \tag{1}$$

where r_i is the radius of the interpolated surface, r_u is the radius of upper surface (leeward side) and r_l is radius of the lower surface (windward side). It is important to note that the interpolating function is only to be used on the interval $\theta \in [-\pi/2, \pi/2]$ and that construction of the interpolated surface in the 2nd and 3rd quadrants of the y-z plane must be made using symmetry in quadrants 1 and 4. Note that a simple linear interpolating function will not satisfy the continuity conditions because a linear function does not contain enough free parameters to satisfy both the position and slope constraints at $\theta = \pm\pi/2$. A cubic polynomial interpolating function; however, will satisfy the four boundary conditions, i.e.

$$\begin{aligned} r_i(\pi/2) &= r_u \\ r_i(-\pi/2) &= r_l \\ \frac{d\lambda}{d\theta}(\pm\pi/2) &= 0 \end{aligned} \tag{2}$$

The general form for a third order interpolating polynomial is given by:

$$\lambda(\theta) = a\theta^3 + b\theta^2 + c\theta + d \tag{3}$$

The coefficients of the polynomial equation must satisfy the following equation:

$$\begin{bmatrix} (\pi/2)^3 & (\pi/2)^2 & (\pi/2) & 1 \\ (-\pi/2)^3 & (-\pi/2)^2 & (-\pi/2) & 1 \\ 3(\pi/2)^2 & 2(\pi/2)^1 & 1 & 0 \\ 3(-\pi/2)^2 & 2(-\pi/2)^1 & 1 & 0 \end{bmatrix} \begin{bmatrix} a \\ b \\ c \\ d \end{bmatrix} = \begin{bmatrix} 1 \\ 0 \\ 0 \\ 0 \end{bmatrix} \tag{4}$$

Solving for the polynomial coefficients one obtains:

$$\begin{bmatrix} a \\ b \\ c \\ d \end{bmatrix} = \begin{bmatrix} -2/\pi^3 \\ 0 \\ 3/(2\pi) \\ 1/2 \end{bmatrix} \tag{5}$$

Substituting the results of Equation 5 back into Equation 1 one can estimate the location of points on the outer mold line in the y-z plane at a given x-station for known values of r_u and r_l via

$$\begin{aligned} y_i &= r_i \cos(\theta) \\ z_i &= r_i \sin(\theta) \end{aligned} \tag{6}$$

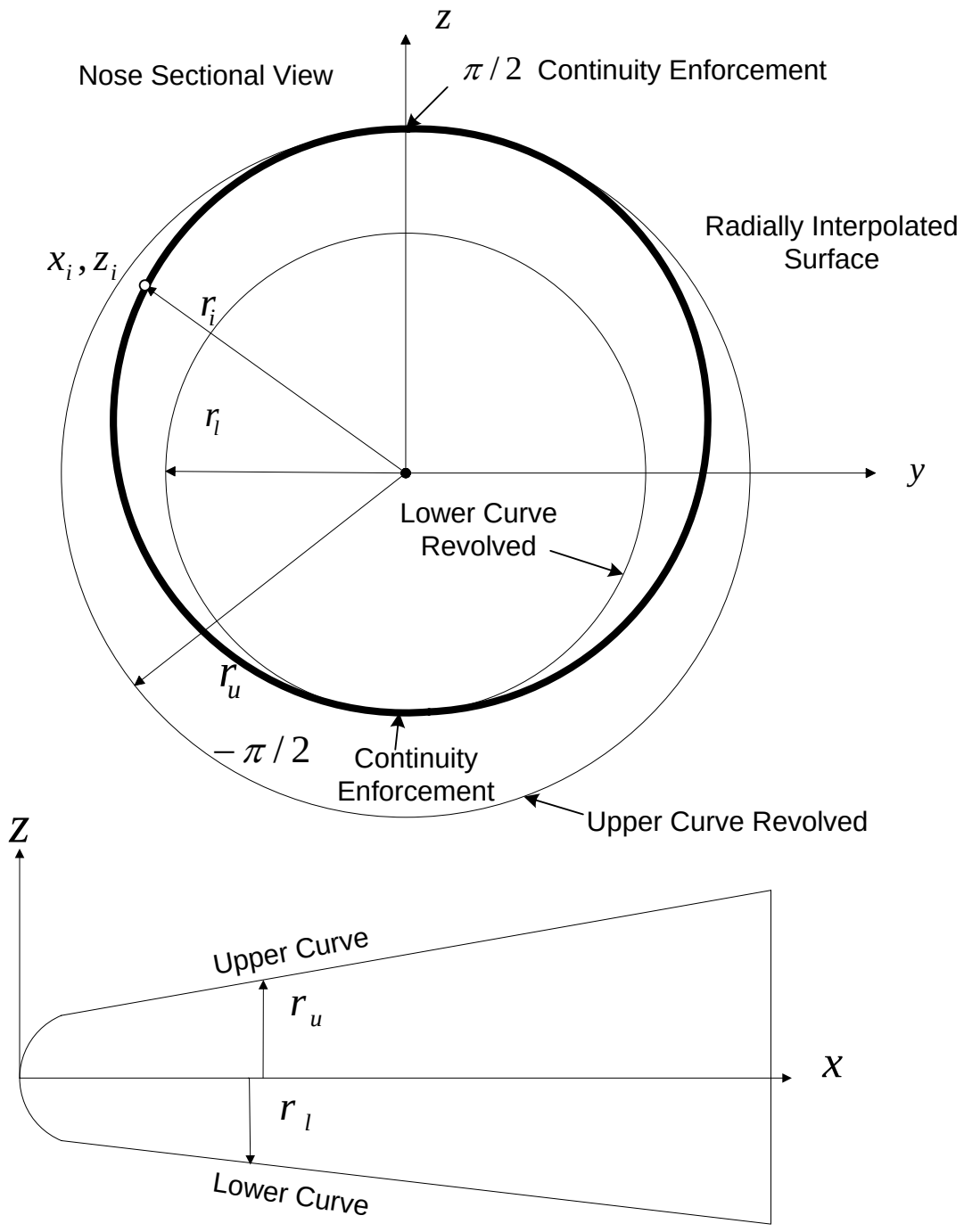

Figure 1. Cubic interpolation between two bodies of revolution

The geometric properties of such an interpolated profile will be of interest in subsequent sections. In particular, the area bounded by the region defined by Equation 1 with polynomial coefficients defined by Equation 5 is given by:

$$A = \int_{-\frac{\pi}{2}}^{\frac{\pi}{2}} r_i^2(\theta) d\theta = \frac{\pi}{35}(13r_l^2 + 13r_u^2 + 9r_u r_l) \tag{7}$$

It will also be useful to compute the volume of regions bounded above and below by surfaces parallel to the y-z plane enclosed by Equation 6 and linearly interpolated in x as shown in Figure 2. Such a region will be used as an estimate of the shape of an ablated vehicle between any two x body axis stations for which data exists in the form of $r_{u_1}, r_{l_1}, x_1, r_{u_2}, r_{l_2}, x_2$. Without loss of generality, we will assume that the base of a section lies at $x_1 = 0$. We can then obtain an expression for the interpolated radius at any location (θ, x) as

$$r_i(\theta, x) = \frac{1}{\Delta x}(r_i(\theta, x_2) - r_i(\theta, 0))(x) + r_i(\theta, 0) \tag{8}$$

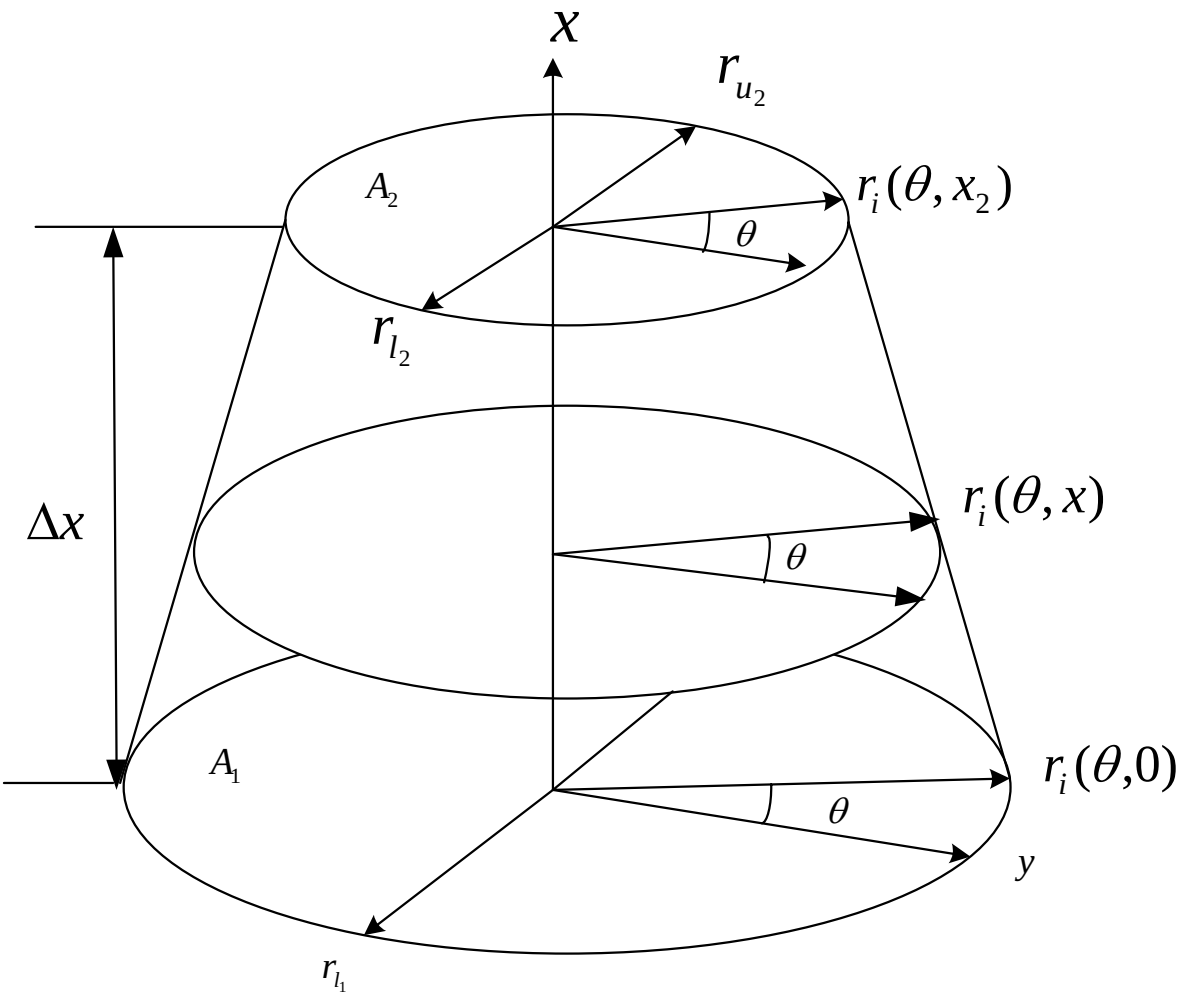

Figure 2. Volume enclosed by a section of interpolated nose cone

The volume of the region can be computed as:

$$V = \int_0^{\Delta x} \int_{-\pi/2}^{\pi/2} r_i^2(\theta, x) d\theta dx \tag{9}$$

Substituting the interpolation coefficients of Equation 5 into Equations 1 and 8 and evaluating the integral one can obtain:

$$V = \frac{\Delta x}{3}\left[A_1 + A_2 + \frac{\pi}{70}[26(r_{u_2}r_{u_1} + r_{l_2}r_{l_1}) + 9(r_{u_2}r_{l_1} + r_{l_2}r_{u_1})]\right] \tag{10}$$

where A_1 and A_2 are the areas of the base and top of the solid respectively.

Finally, the reader should be advised that there are limitations of the cubic radial interpolation function used in this application. In order for the interpolation function to produce a physically meaningful result at a given x-station, the lower radius must be no less than about 38% of the upper radius or more precisely,

$$r_l \geq \frac{6}{\pi^2 + 6} r_u \tag{11}$$

If this relationship is not satisfied, then the cubic interpolation function will result in cusped cross-section. The above relationship can be found by using a 2nd derivative test for a critical point at $\theta = -\pi/2$, i.e.

$$\left.\frac{d^2z}{dy^2}\right|_{\frac{-\pi}{2}} = \left.\frac{d^2z}{d\theta^2}\frac{d^2\theta}{dy^2}\right|_{\frac{-\pi}{2}} = 0 \tag{12}$$

Defining $r_l = kr_u$ and substituting Equation 1 into Equation 12, one obtains:

$$0 = \left.\frac{d^2z}{d\theta^2}\right|_{\frac{-\pi}{2}} = \left.\frac{d^2\left[\lambda(\theta)r_u + (1-\lambda(\theta))\right]kr_u]\,sin(\theta)}{d\theta^2}\right|_{\frac{-\pi}{2}} \tag{13}$$

evaluating Equation 13 and solving for k yields,

$$k = \frac{6}{\pi^2 + 6} \tag{14}$$

□

For cases where the windward vehicle surface ablates significantly more than the leeward surface, the reader is advised to check this condition at each x-station to ensure that the interpolation function provides a physically meaningful OML.

III. Computing Instantaneous Mass of Nose Cone

First we will assume that the nose cone density ρ_n is constant throughout. It is also assumed that test data is available that provides the upper and lower curves for one or more ablated cases. The volume and thus the mass of the ablated and unablated nose cones can computed using the 3-D OMLs generated using the techniques described in the previous section. The following formula for predicting mass loss rates due to ablation has been proposed:[3]

$$\frac{dm}{dt} = -\frac{C_H}{H}\frac{1}{2}\rho V^3 S \tag{15}$$

where m is the mass of the nose cone, C_H is a dimensionless heat transfer coefficient less than unity, H is the effective heat of ablation, ρ is the air density, V is the velocity of the body with respect to the air mass, and S is the current cross sectional frontal area of the body. Note that C_H and H are vehicle and material dependent parameters and we hereby denote the ratio C_H/H as K_H. Equation 15 can be integrated over trajectory to obtain:

$$m_f - m_i = -\frac{1}{2}K_H S \int_0^t \rho(t)V(t)^3 dt \tag{16}$$

where m_f and m_i are the initial and final values of the nosecone mass. Denoting $\Delta m = m_f - m_i$ and solving for K_H we have:

$$K_H = 2\frac{\Delta m}{S\int_0^t \rho(t)V(t)^3 dt} \tag{17}$$

Estimates of ρ can be obtained from an atmospheric model, V can be measured or estimated from test instrumentation, and changes in mass can be determined from recession measurements. Thus, Equation 17 can be used to empircally estimate K_H for the flight profile for which the recession measurements were obtained. The integral is not analytically tractable; however, it can be evaluated by quadrature.

IV. Interpolating Outer Mold Lines

While the centroid and elements of the inertia tensor of the nose cone can change significantly as a result of ablation, those effects usually have little influence upon the mass properties of the vehicle as a whole. In some cases the changes in mass properties due to ablation can be neglected for the purposes of flight simulation. Nevertheless, computation of the OML based on instantaneous mass is still important because the aerodynamic properties are a strong function of the OML. Since the aerodynamic properties are primarily influenced by OML, and OML and mass are related, a method is proposed that will allow the aerodynamic characteristics of an ablated profile to be estimated using using instantaneous mass as an interpolation variable.

Generally, a small number of OMLs are known from test or prediction data. We would like to estimate the shape and aerodynamic characteristics of the vehicle based on measurements or predictions of a finite number of OMLs and estimates of instantaneous mass. During a simulation run, the time rate of change of vehicle mass due to ablation can be computed dm/dt via Equation 15. Thus the mass of the vehicle can be computed as a function of time in a dynamic simulation. Given the masses associated with known OMLs, it is desired to estimate the instantaneous OML location and the associated aerodynamic characteristics for any specified mass. In order to obtain a point on an OML for a given mass, one must interpolate between two points on adjacent OMLs defined by test or prediction data. Numerous choices exist for selecting match points on the inner and outer surfaces. Here we propose to match points on adjacent OMLs that have equal slopes. This choice is motivated by Newtonian flow considerations wherein the local temperature and pressure on a body are dictated by the local surface inclination measured with respect to the freestream,[4] i.e.

$$\begin{aligned} \frac{T_2}{T_\infty} &= \frac{2\gamma(\gamma-1)}{(\gamma+1)^2} M_\infty^2 \sin^2\beta \\ \frac{P_2}{P_\infty} &= \frac{2\gamma}{\gamma+1} M_\infty^2 \sin^2\beta \end{aligned} \tag{18}$$

where β is the angle between a tangent line on a surface and the freestream. We therefore propose to interpolate along lines connecting points on the inner and outer surfaces that have equal surface inclination angles as illustrated in Figure 3. Points on the interpolated OML are computed as follows:

$$\begin{aligned} x_{OML} &= \lambda_m(m) x_i + (1-\lambda_m(m)) x_o \\ z_{OML} &= \lambda_m(m) z_i + (1-\lambda_m(m)) z_o \end{aligned} \tag{19}$$

where $\lambda_m(m) \in [0,1]$ is an interpolation function that relates changes in distance to changes in the instantaneous mass of the vehicle. In cases where discontinuities arise because segments of one OML do not have slopes that match those on adjacent surface, such points are matched to a corner point on an adjacent OML as illustrated in Figure 3.

Since mass or volume is a cubic function of the linear dimensions of a body, one might postulate the following form for the interpolation function:

$$\lambda_m(m) = K_1 m^{\frac{1}{3}} + K_2 \tag{20}$$

Clearly $\lambda_m(m_o) = 0$ and $\lambda_m(m_i) = 1$, thus

$$\begin{aligned} K_1 &= \frac{1}{m_i^{\frac{1}{3}} - m_o^{\frac{1}{3}}} \\ K_2 &= \frac{-m_o^{\frac{1}{3}}}{m_i^{\frac{1}{3}} - m_o^{\frac{1}{3}}} \end{aligned} \tag{21}$$

The distance that a point moves along a line connecting the inner and outer control points is therefore assumed to be related to the cube root of the volume or mass. The above relationship would yield accurate results for an object that ablated symmetrically in all directions; however, ablation on reentry vehicles is typically asymmetric. One should therefore judiciously select an interpolation function that correlates changes in mass with changes in OML location. For example, if an unablated body is a cylinder capped by

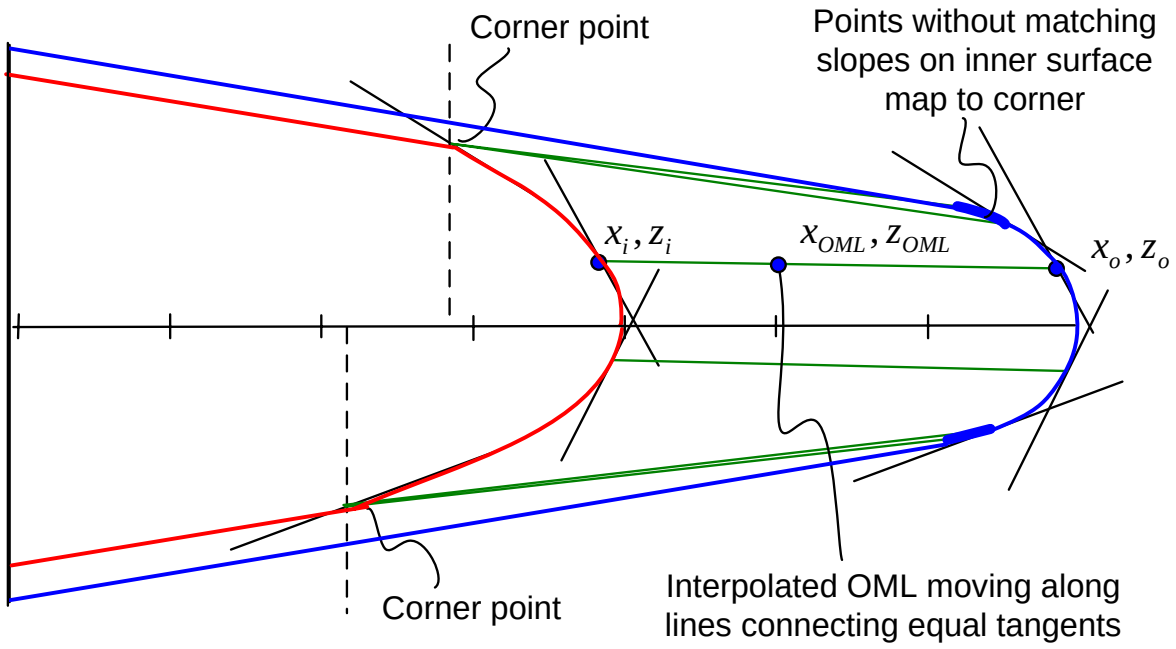

Figure 3. OML Interpolation based on instantaneous mass

a hemisphere and held at zero angle of attack in a hypersonic flow, one would expect the principle change in geometry to be in the length of the body with perhaps a slight change in radius. Since the mass or volume of such a body is a linear function of length, one would expect that a linear interpolation function would be an appropriate choice for relating changes in mass to OML location.

$$\lambda_m(m) = K_1 m + K_2 \tag{22}$$

$$\begin{aligned} K_1 &= \frac{1}{m_i - m_o} \\ K_2 &= \frac{-m_o}{m_i - m_o} \end{aligned} \tag{23}$$

In general,

$$\lambda_m(m) = K_1 f(m) + K_2 \tag{24}$$

where $f(m)$ is a function that correlates mass and OML location, and the coefficients, K_1 and K_2 are computed from the boundary conditions $\lambda_m(m_o) = 0$ and $\lambda_m(m_i) = 1$.

The interpolation of aerodynamic tables using instantaneous mass proceeds along similar lines since the aerodynamic properties are significantly influenced by OML. Typically aerodynamic force and moment coefficients are tabulated as a function of angle-of-attack, sideslip angle, Mach number and control surface deflections. For a vehicle that experiences ablation, the aerodynamic data will also be a function of the instantaneous outer mold line of the vehicle. Thus, additional aerodynamic tables can be constructed for a representative set of ablated OMLs. Between the table break points established for given or estimated OMLs it is proposed that the tables be interpolated using the interpolation function that is used to compute OML location based on mass, i.e. Equation 24, because of the strong influence of OML on aerodynamic coefficients. For an arbitrary aerodynamic coefficient the following interpolation scheme is proposed:

$$C_x(M, \alpha, \beta, \boldsymbol{\delta}, m) = \lambda(m) C_x(M, \alpha, \beta, \boldsymbol{\delta}, m_i) + [1 - \lambda(m)] C_x(M, \alpha, \beta, \boldsymbol{\delta}, m_o) \tag{25}$$

In summary, to interpolate the aerodynamic tables, one must estimate the instantaneous mass of vehicle using Equation 15, and use an interpolation function given by Equation 24 in conjunction with Equation 25.

V. Prediction of Aerodynamic Properties from Outer Mold Lines

Many design codes exist that can predict the aerodynamic characteristics of blunted bodies at high speeds. Newtonian theory has been shown to provide good lift and pitching moment predictions for a variety of sharp and blunted body shapes at Mach numbers as low as 2.75.[5] Addition of viscous effects (skin friction, base drag) improves the accuracy of drag predictions. Newtonian impact theory ($C_p = 2\sin^2\delta$) typically provides reasonable agreement for sharp cones. The modified form of Newtonian theory, where the pressure coefficient of 2 is replaced by the stagnation pressure behind a normal shock, has been shown to give better results for highly blunted configurations.

Although Missile Datcom[6] contains a Newtonian flow option, it was not selected for the analysis of the example body presented in the subsequent section, because it is limited to bodies of circular or elliptic cross-section, and the cross-section shapes resulting from the proposed ablateness model are neither. In addition, the Newtonian formulation[7] used by Missile Datcom does not include the axial force contribution to pitching moment (a common simplification). The code selected for the present analysis is a modified version of the Low Observable Design Synthesis Tool[8] (LODST), which was developed for analysis of arbitrary body missiles. LODST has a geometry modeler suitable for shapes generated by the proposed ablateness model, and also contains a Newtonian flow calculation. Both of these were taken from the Supersonic/Hypersonic Arbitrary Body Program,[9] a widely used code. The Newtonian flow calculations were isolated from the slender body theory calculations within LODST, and base drag and skin friction calculations were added using methods from Missile Datcom.

Many databases exist on blunted cones at high speeds. Neal[10] tested several configurations at a Mach number of 6.77, one of which is similar to the configuration considered in the subsequent example. The length to base diameter ratio of the configuration considered in the example in the next section decreases from 1.52 to 0.98 as the nose ablates. In order to validate the accuracy of the predictions for the example problem, we compare results obtained from the LODST code to test data. The comparable ratio of the configuration tested by Neal is 1.38. The ratio of the nose bluntness radius to base radius of the example configuration increases from 0.44 to 0.73 as the nose ablates. The comparable ratio of the configuration tested by Neal is 0.66. The LODST representation of the Neal configuration is shown in Figure 4. A comparison of the axial force coefficient predicted by LODST with test data is shown in Figure 5. The agreement is excellent when the viscous contribution is added to the modified Newtonian result. Normal force comparisons are shown in Figure 6. Again, the agreement is excellent for the modified Newtonian prediction.

VI. Example

Consider the unablated nose cone of a reentry vehicle shown in Figure 7 that consists of a 12 deg conical frustrum capped by a zone of a sphere of radius 1. More precisely the outer mold lines in the x-z plane are given by:

$$z(x) = \pm\sqrt{1-x^2}, \qquad \cos(78^o) \le x \le 1 \tag{26}$$

$$z(x) = \pm[\tan(12^o)x - (\sin(78^o) + \tan(12^o)\sin(12^o))], \qquad -6 \le x \le \cos(78^o) \tag{27}$$

Suppose that at a certain stage in a flight, a recession sensor suite has provided measurements of the ablated nose cone in the x-z plane that has the geometry represented by inner curves shown in Figure 7 which are described as follows:

$$z_u(x) = \sqrt{-2(x+2)}, \qquad -3.096 \le x \le -2 \tag{28}$$

$$z_u(x) = [-\tan(12^o)x + (\sin(78^o) + \tan(12^o)\sin(12^o))] - .2, \qquad -6 \le x \le -3.096 \tag{29}$$

$$z_l(x) = -\sqrt{\frac{-4}{3}(x+2)}, \qquad -3.714 \le x \le -2 \tag{30}$$

$$z_l(x) = [\tan(12^o)x - (\sin(78^o) + \tan(12^o)\sin(12^o))] + .3, \qquad -6 \le x \le -3.714 \tag{31}$$

Based on the outer-mold-lines measured in the x-z plane and an estimate of the instantaneous mass of the nose cone it is desired to estimate the instantaneous aerodynamic properties and OML location. This is accomplished by using Equations 19 and 25. Points on the ablated and unablated surfaces whose tangents are equal are used in Equation 19, thus, mass interpolated points on the OML in the x-z plane proceed along

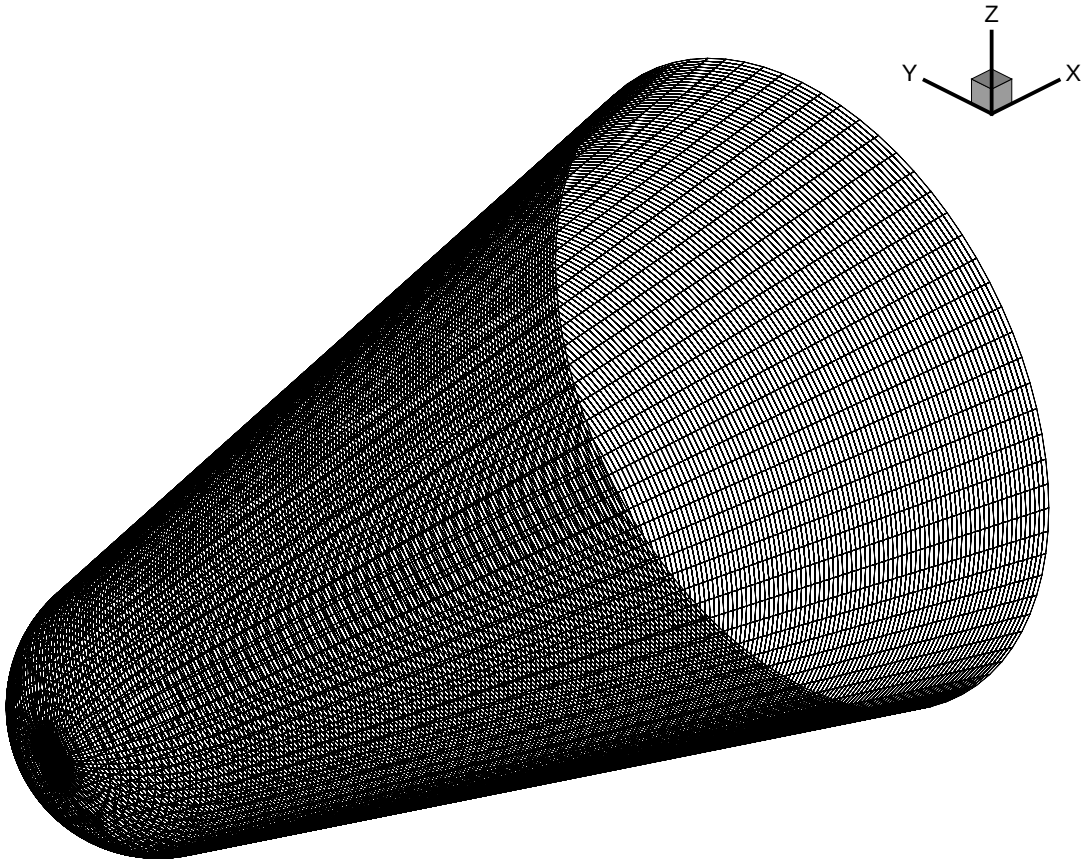

Figure 4. LODST Grid for Neal Configuration

the equi-tangent lines shown in Figure 8. Figure 9 shows the estimated outer mold line locations associated with specified values of the mass interpolation function given by Equation 24.

For a given value of nose cone mass, mass interpolated curves in the x-z plane for the upper and lower surfaces can be generated as described above and one can use Equations 1 and 6 to estimate out-of-plane grid points that are suitable for use with CFD or an aerodynamic prediction code such as LODST. The 3-D OML of the ablated body is shown in Figure 10. Upon generating such a grid, the aerodynamic properties can be estimated using CFD or prediction codes such as LODST. The actual volume or mass of the interpolated body can be calculated by discretizing the along the x-body axis and summing the volumes of each section given by Equation 10. In this example, we assume that the nose cone material is homogenous with unit density, thus the magnitudes of the volume and the mass are equal. Mass calculations can be used to assess the adequacy of basis functions chosen for the mass interpolation. The effectiveness of the outer-mold line interpolation method can be assessed by specifying a value for the interpolation function λ, estimating the outer mold line location and then calculating the mass of the body described by the resulting outer mold line. The mass of the example body, which we will call the actual mass (m_a), was calculated for a number of values of λ. The result is shown in Figure 11 and represents the shape of the ideal interpolating function for the geometry under consideration. When choosing a basis function for Equation 24 one can evaluate the effectiveness of the choice by comparing the relationship between mass and λ for a given form of interpolation function to the ideal result. The mass associated with a specified value of λ can be obtained

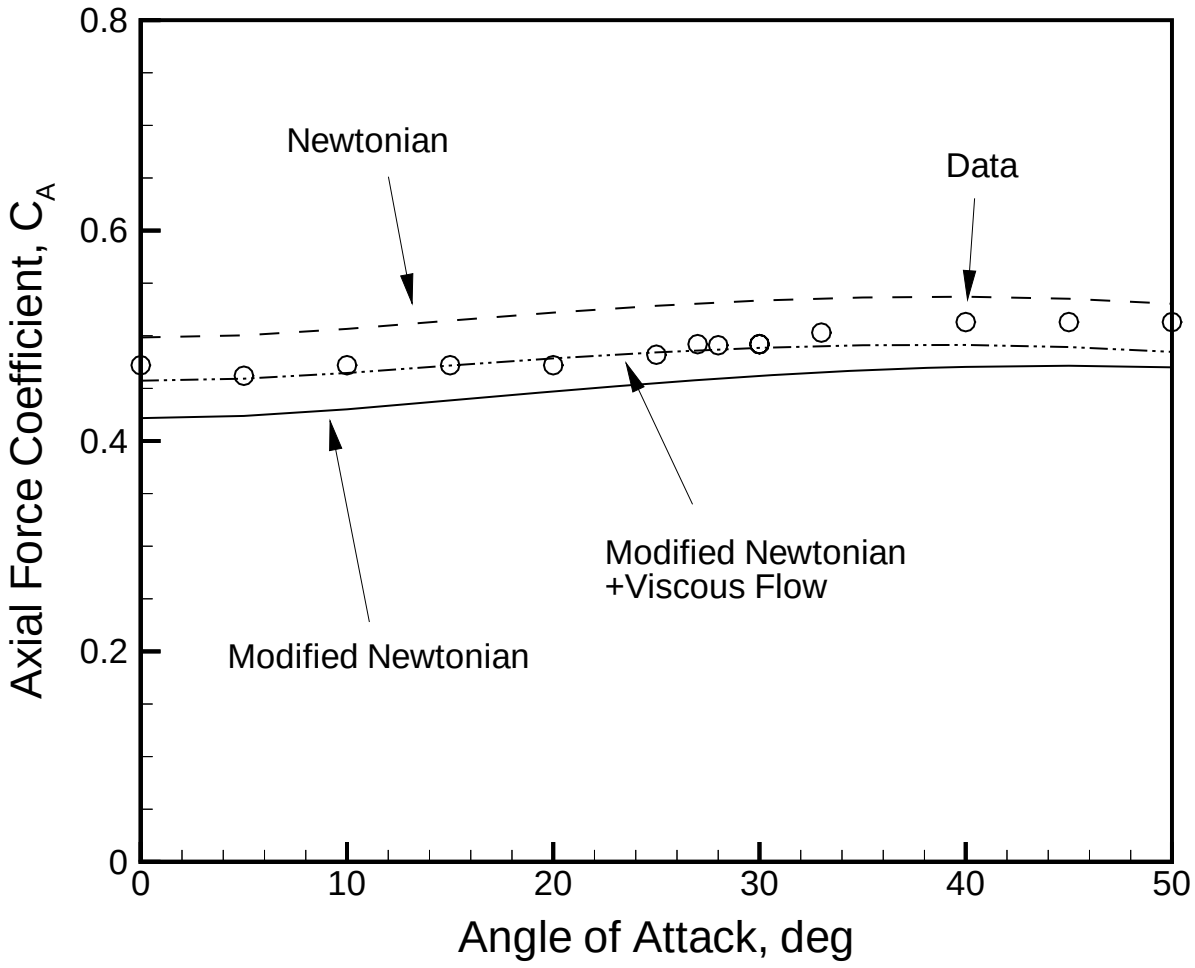

Figure 5. Axial Force Comparision for Neal Configuration

by solving Equation 24 for m which we will define as m_s:

$$m_s \equiv f^{-1}\left[\frac{\lambda - K2}{K1}\right] \tag{32}$$

From Figure 11, one can see that the linear and cube-root interpolation methods only agree with the ideal or actual values at the boundary conditions (i.e. unablated and fully ablated conditions) and that the linear interpolation method is superior to the cube-root result in this particular case. In this example, we note that the primary change in mass is due to a change in length along the x-axis and that there is relatively little change in the radial direction. Thus, representing the change in outer mold line location as a linear function of mass, yields superior results to using cube-root interpolation since the major changes to linear dimensions of the body occur along a single direction. If a body ablated uniformly in all directions, one would expect the cube-root based interpolator to produce superior results. In order to alleviate computational burden, it is desirable to avoid running CFD or aerodynamic prediction codes at every time-step in a 3 or 6 degree of freedom dynamic flight simulation. Thus using Equation 25 to estimate aerodynamic properties is preferable to generating OML grids and running prediction codes as the simulation progresses even though it is expected that the latter would produce more accurate results. A good choice of interpolation basis function can reduce these inaccuracies. To illustrate this point we use LODST to predict the lift, drag and pitching moments of the ablated and unablated bodies at Mach = 10 and $\alpha = 10^o$. Here we are interested in assessing how well a mass interpolated (i.e. Equation 25) aerodynamic prediction matches the LODST prediction for OMLs

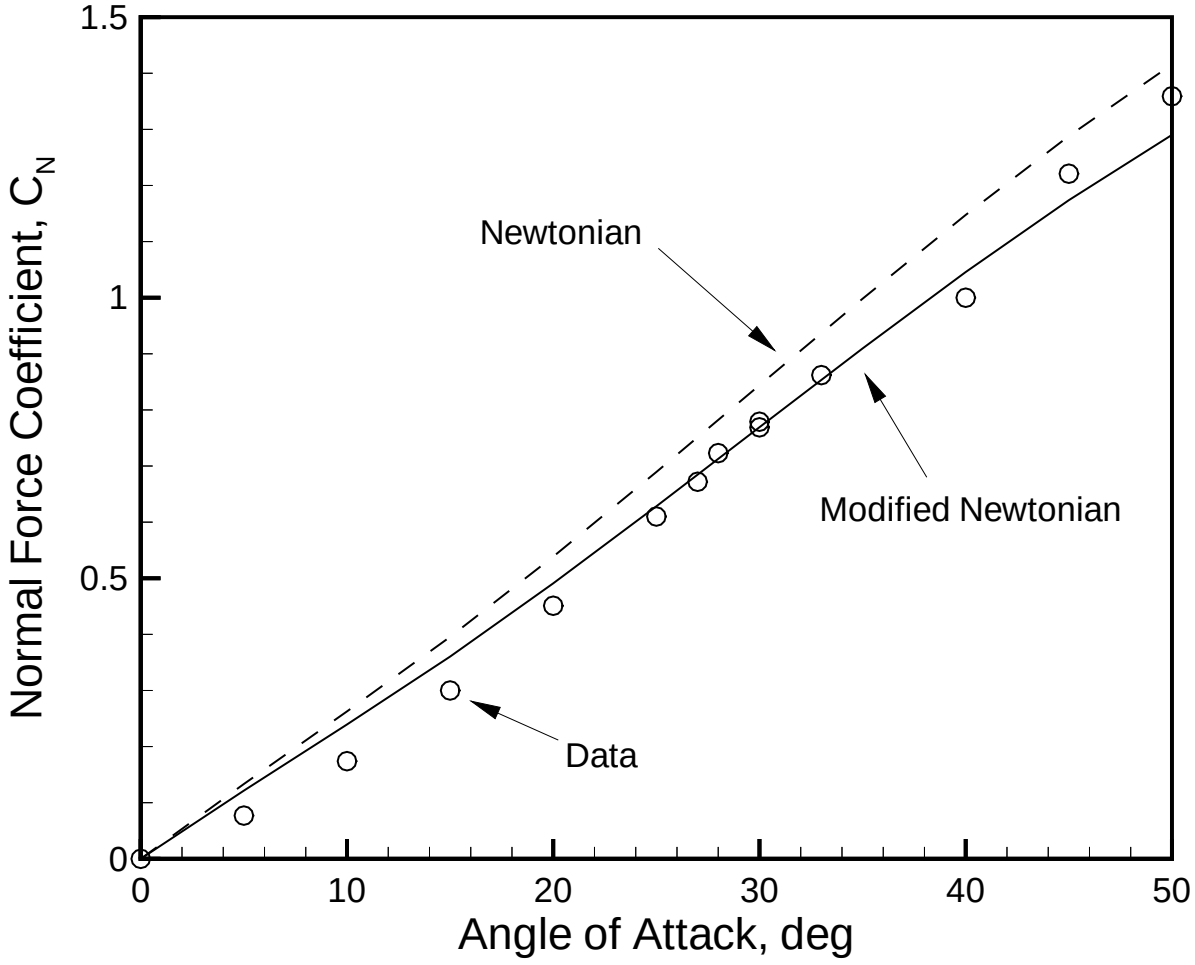

Figure 6. Normal Force Comparision for Neal Configuration

associated with a specified mass. For the purposes of this exercise, we take the LODST prediction to be the "actual" value of the aerodynamic coefficient which we use to assess the accuracy of Equation 25 for both cube-root and linear interpolation methods. Figures 12 and **??** show how the lift and drag of the example body change as a function of mass. Note that there are two sources of error associated with the interpolated results on these figures. The first source of error is that there is a difference between the interpolated value of mass and the actual mass of the body described by the OML grid, i.e. $m_s - m_a \neq 0$. The second source of error arises because the interpolation basis functions do not yield exact results at points other than the boundary conditions. This example shows a rather extreme case where there is a large difference between two known OMLs. In practice the differences between known OMLs is generally much smaller, making the choice of interpolation basis functions less critical. Even in cases where large differences exist between known OMLs, the use of OML interpolation in conjunction with prediction codes can be used to obtain more accurate estimates of aerodynamic coefficients and mass between test data points in order to augment table lookup data for dynamic simulation purposes.

VII. Summary

A method for estimating the effects of nose cone ablation on the aerodynamic forces and moments of a reentry vehicle has been presented. The method provides a means of generating a rough, but representative model that makes use of interpolated test or prediction data using instantaneous nose cone mass as an inter-

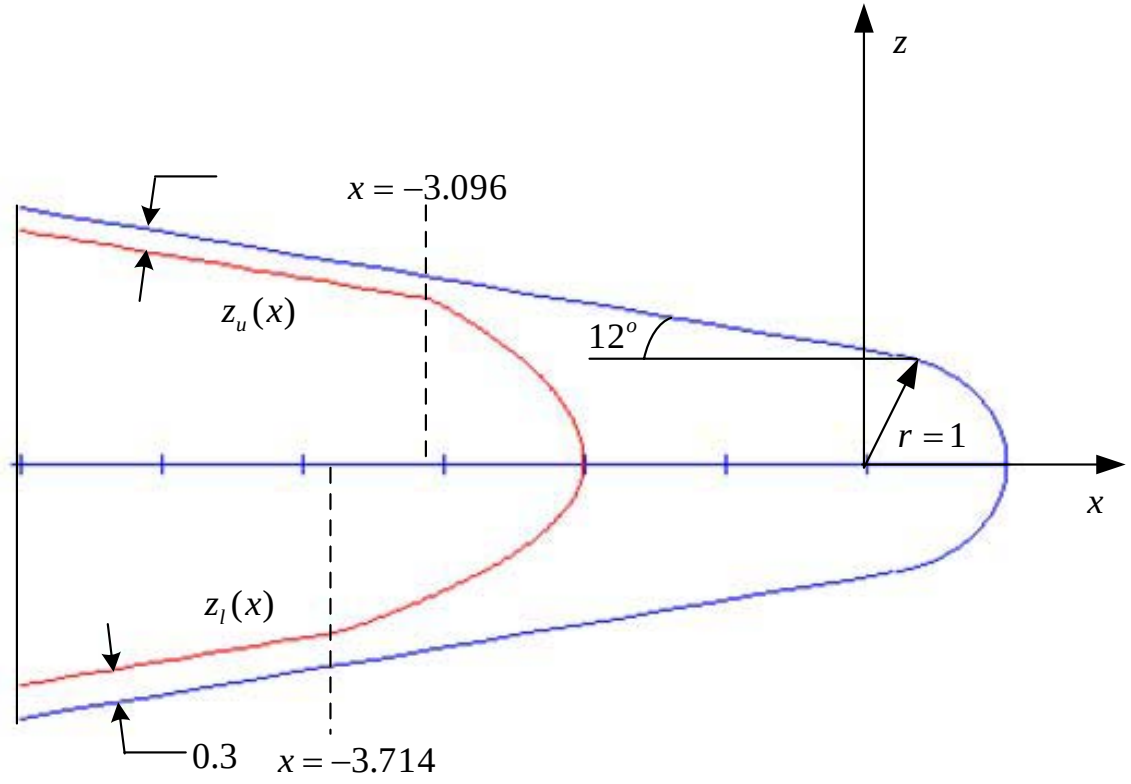

Figure 7. Example Geometry of an Ablated and Unablated Nose Cone

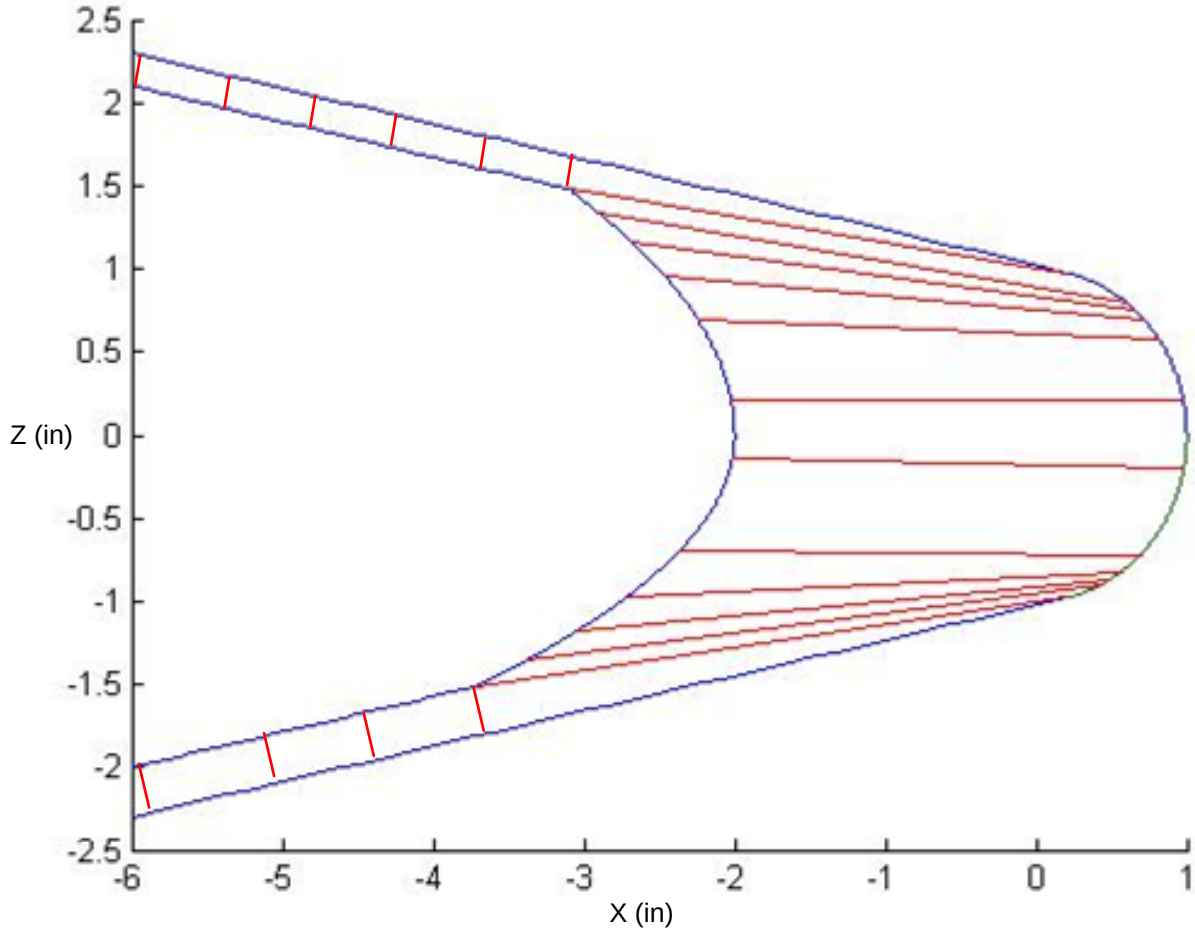

Figure 8. Lines connecting points of equal tangents on ablated and unablated surfaces

polation variable. Since aerodynamic properties are strongly influenced by outer-mold-line, an interpolation function was proposed that can be used to approximate the location of points on the outer-mold-line as well as the aerodynamic characteristics test points. While the changes in overall vehicle mass properties due to ablation are typically small, one can make use of the interpolated outer-mold-line information to estimate mass properties, such as moments of inertia or center of gravity. The interpolated aerodynamic and mass properties provide a means for generating data for dynamic simulations for use in vehicle proof-of-concept studies.

References

[1]Noffz, G. K. and Bowman, M. P., "Design and Laboratory Validation of a Capacitive Sensor for Measuring the Recession of a Thin-Layered Ablator," Tech. Rep. NASA TM-4777, NASA Dryden Flight Research Center, Edwards, CA, 1996.

[2]Brandson, G. and Davis, W., "Heat-shield Ablation and Sublimation Determinations Through Radioisotope Techniques," *Proc. 2nd AIAA Annual Meeting*, No. 65-362, AIAA, July 1965.

[3]Loh, W. H. T., editor, *Re-entry and Planetary Entry Physics and Technology*, chap. Gazley, C., Jr., "Entry Deceleration and Mass Change of an Ablating Body", Springer-Verlag, New York, 1968, pp. 415–435.

[4]Anderson, J. D., *Hypersonic and High Temperature Gas Dynamics*, AIAA, Reston, VA, 2000, pp. 33–34.

[5]Dennis, D. and Cunningham, B., "Forces and Moments on Pointed and Blunt-Nosed Bodies of Revolution at Mach numbers from 2.75 to 5.00," Tech. Rep. RM A52E22, NACA, Aug. 1965.

[6]Blake, W. B., "Missile Datcom User's Manual - 1997 FORTRAN 90 Revision," Tech. Rep. VA-WP-TR-1998-3009, AFRL, WPAFB, OH, Aug. 1998.

[7]Rainey, R., "Working Charts for Rapid Prediction of Force and Moment Pressure Coefficients on Arbitrary Bodies of

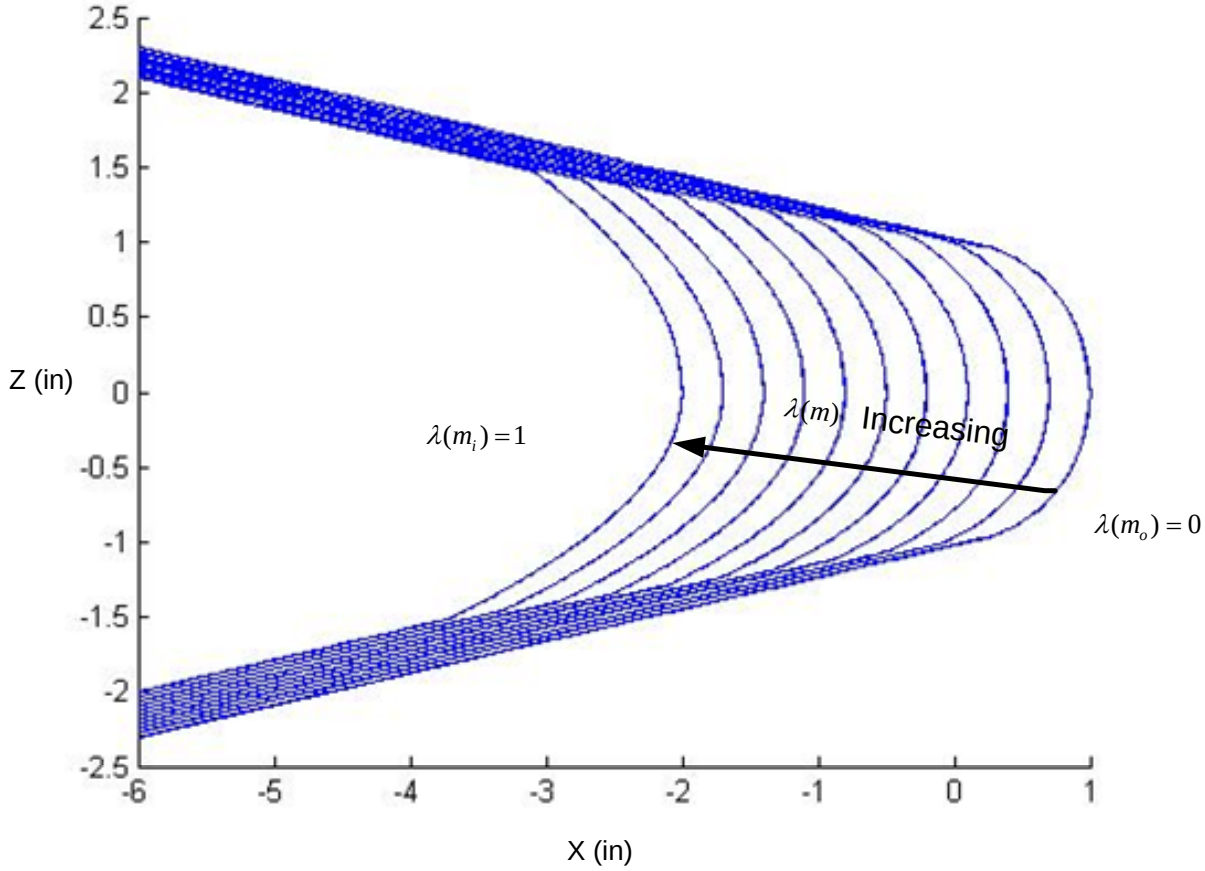

Figure 9. Example of interpolated outer mold lines in x-z plane.

Revolution by Use of Newtonian Concepts," Tech. Rep. TN D-176, NASA, Dec.

[8]Bennett, B., "Conceptual Design Synthesis Tool for Arbitrary Body Missiles ," *Proceedings of the 1997 Applied Aerodynamics Conference*, AIAA 1997-2281, June 1997.

[9]A.E. Gentry, D. S. and Oliver, W., "Supersonic/Hypersonic Arbitrary Body Program," Tech. Rep. TR-73-159, AFFDL, WPAFB, OH, Nov. 1973.

[10]Neal, L., "Aerodynamic Characteristics at a Mach Number of 6.77 of a 9^o Cone Configuration, With and Without Spherical Afterbodies, at Angles of Attack up to 180^o with Various Degrees of Nose Blunting"," Tech. Rep. TN D-1606, NASA, Mar. 1963.

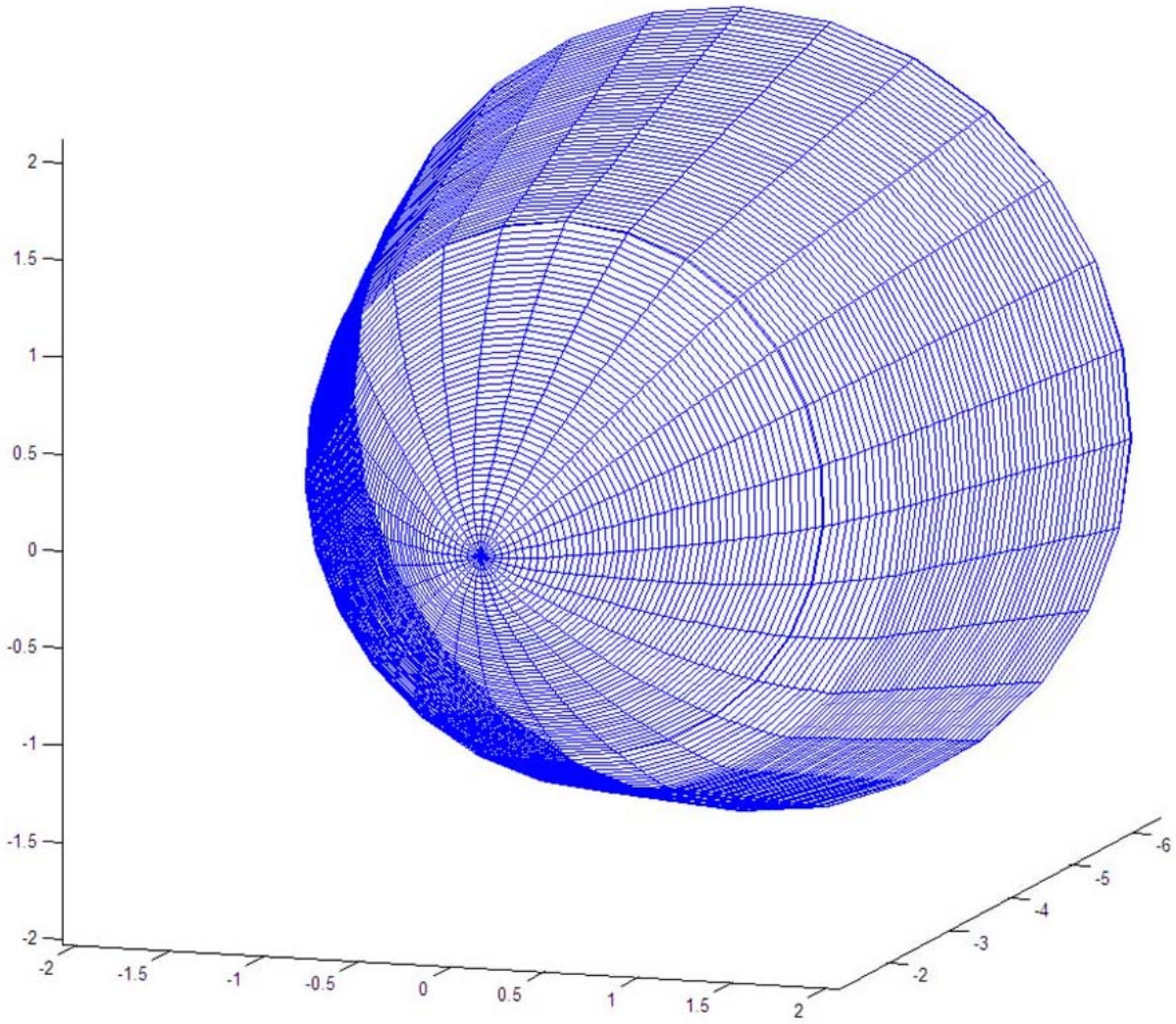

Figure 10. Grid of points on ablated OML using radial interpolation.

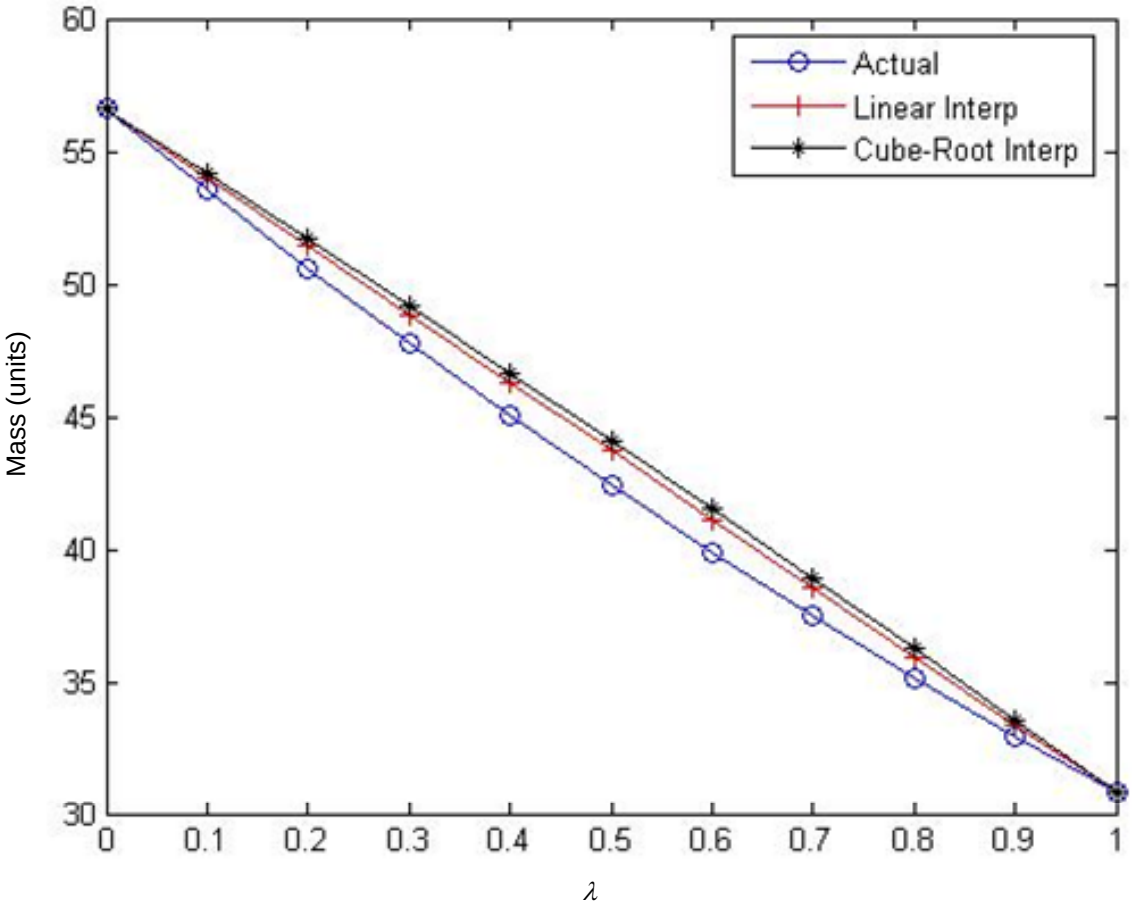

Figure 11. Mass versus interpolation function value

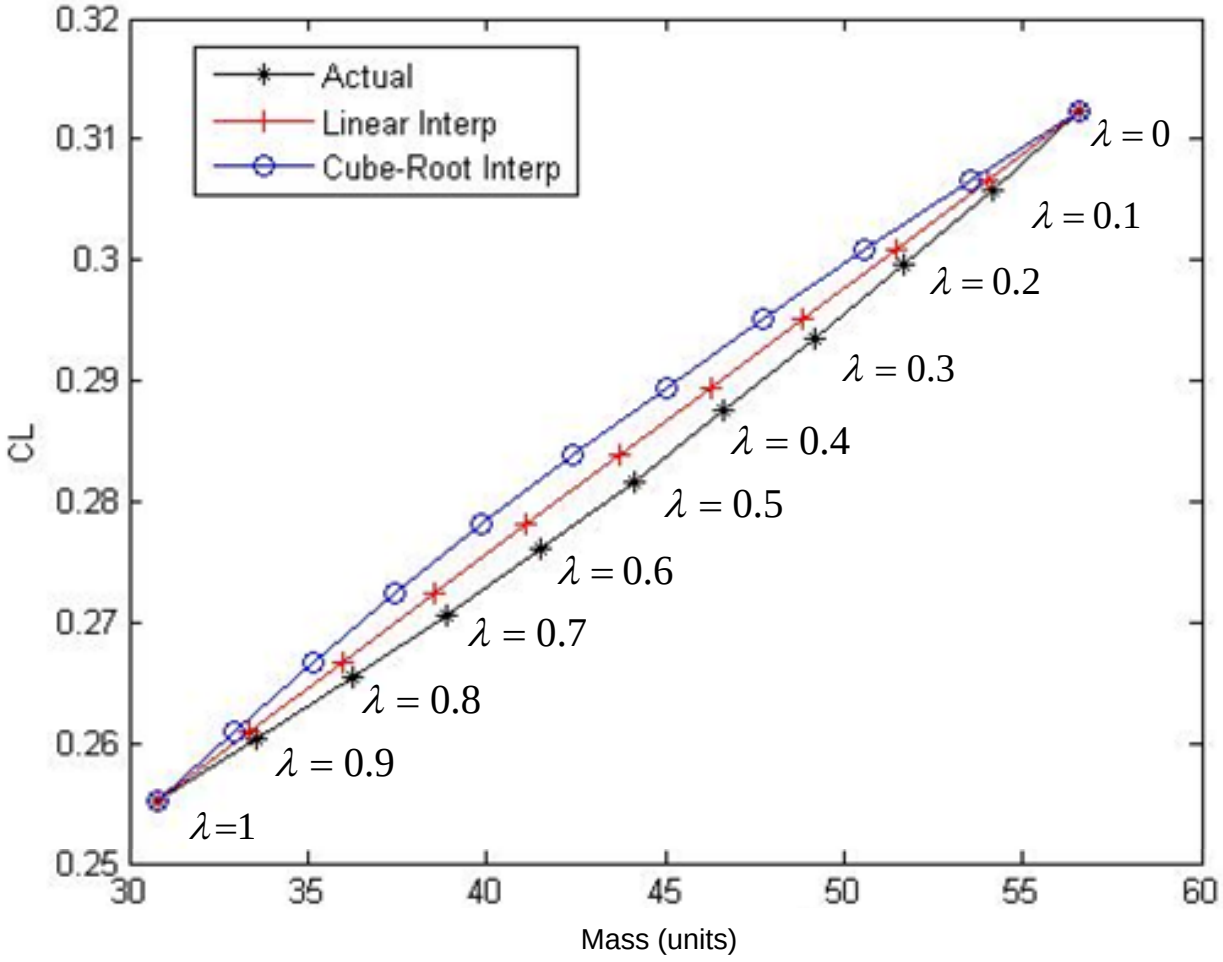

Figure 12. Predicted lift coefficient variations due to mass

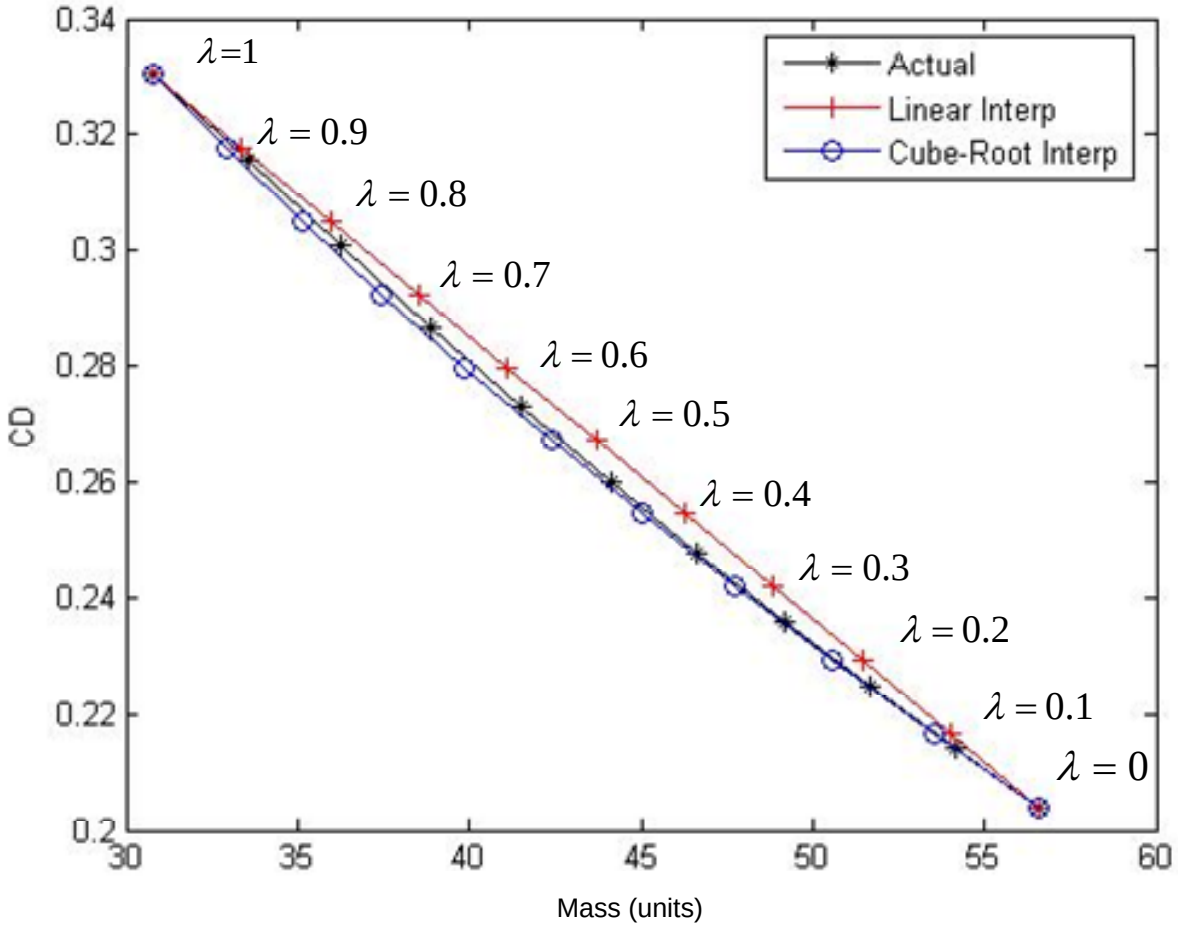

Figure 13. Predicted drag coefficient variations due to mass